View metadata, citation and similar papers at core.ac.uk

brought to you by CORE

provided by University of Johannesburg Institutional Repository

Energy Conversion and Management 64 (2012) 328–334

Contents lists available at SciVerse ScienceDirect

Energy Conversion and Management

journal homepage: www.elsevier.com/locate/enconman

The effects of perforation sizes on laminar heat transfer characteristics of an array of perforated fins

Mohammad Reza Shaeri, Tien-Chien Jen *

Department of Mechanical Engineering, University of Wisconsin – Milwaukee, Milwaukee, WI, USA

ARTICLE INFO

Article history:
Received 19 September 2011
Received in revised form 30 April 2012
Accepted 1 May 2012
Available online 27 September 2012

Keywords:
Perforated fin
Heat transfer enhancement
Laminar flow
Convection heat transfer

ABSTRACT

Shaeri and Yaghoubi [25] reported the highest heat transfer rate in a laminar flow for a perforated fin with the most perforations (porosity), regardless of investigation on the effects of perforation sizes. In this study, the effects of size and number of perforations on laminar heat transfer characteristics of an array of perforated fins at the highest porosity of the study of Shaeri and Yaghoubi [25] have been numerically investigated. The Navier–Stokes and energy equations are solved by the finite volume procedure using the SIMPLE algorithm. Results show that at a specific porosity, the thermal entrance length of each perforation of a fin with a lower number of perforations is larger than that of each perforation of a fin with a higher number of perforations. Therefore, in a laminar flow and at a constant porosity, a fin with fewer perforations is more efficient to enhance the heat transfer rate compared with a fin with more perforations. Although perforated fins have higher friction drag and lower pressure drag with respect to solid fins, perforated fins do not affect total drag.

© 2012 Elsevier Ltd. All rights reserved.

1. Introduction

Extended surfaces, or fins, used as powerful tools to exchange heat between a primary surface and ambient fluid have been applied in almost all industries that use heat exchangers; therefore, many attempts have been made to design optimized fins. Fin optimization is defined as either reducing the weight of a fin at a specific heat removal or increasing the heat removal at a specific fin weight [1]. Studies regarding fin optimization are extensive and several can be found in [1–16]. The use of perforated fins has been considered as one of the most useful methods in fin optimization; in fact, due to perforations, by increasing heat transfer area in one area and reducing fin weight on the other area, both goals of fin optimization can be achieved simultaneously.

Souidi and Bontemps [17] considered both plain and perforated fins in narrow rectangular channels and experimentally investigated the flow insides the channels. Sara et al. [18] and Sahin and Demir [19] reported enhanced heat transfer from a flat surface in a channel flow by using perforated blocks with rectangular cross-sections. The same results also were obtained by using perforated fins with circular cross-sections in the study of Sahin and Demir [20]. Karabacak and Yakar [21] experimentally investigated the effects of angular locations of holes on perforated fins. According to their study, at Reynolds numbers above the critical value, the Nusselt number was higher for perforated fins compared with imperforated fins. Karabacak and Yakar [21] also proposed a correlation between Reynolds and Nusselt numbers.

Shaeri et al. [22] and Yaghoubi et al. [23] studied the heat transfer characteristics of an array of perforated fins, where perforations were on the lateral surfaces of fins in a turbulent and laminar flow, respectively. Although in both [22,23] enhanced heat transfer was not achieved, considerably lighter fins were obtained without any penalty in the heat transfer rate. Shaeri and Yaghoubi [24,25] numerically studied the heat transfer characteristics of arrays of rectangular perforated fins in turbulent and laminar flows in which perforations were located along the length of fins. In both studies [24,25], the authors defined porosity as the emptied volume of the fin due to perforations divided by the fin volume without perforations. Shaeri and Yaghoubi [24,25] reported that a perforated fin with the highest porosity provides the most enhanced heat transfer rate.

The present study is a supplement to the study by Shaeri and Yaghoubi [25] to investigate the effects of perforati Re_D on sizes on the laminar heat transfer characteristics of an array of perforated fins, in which the perforated fin with the highest porosity in [25] is selected and its heat transfer characteristics are investigated by changing both the numbers and sizes of the perforations while the porosity remains unchanged. Then, the obtained results are compared with those of the solid fin and the fin with the highest porosity in [25].

* Corresponding author. Tel.: +1 414 229 2307; fax: +1 414 229 6958.
E-mail address: jent@uwm.edu (T.-C. Jen).

0196-8904/$ - see front matter © 2012 Elsevier Ltd. All rights reserved.
http://dx.doi.org/10.1016/j.enconman.2012.05.002

Nomenclature

ΔA	area (m^2)
A_F	fin area that is touched by air in flow direction (m^2)
A_P	frontal area of fin (m^2)
C_p	specific heat at constant pressure ($J\ kg^{-1}\ K^{-1}$)
D, H, L, S_F	fin thickness, height, length and spacing, respectively (m)
D_h	hydraulic diameter of the duct in [29] (m)
F_F, F_P, F_D	friction, pressure and total drag, respectively (N)
$h, \bar{h}$	local and average convection heat transfer coefficient, respectively ($W\ m^{-2}\ K^{-1}$)
H_b, H_d	block and duct heights, respectively, in [29] (m)
H_p, W_p	perforation height and width, respectively (m)
K	thermal conductivity of fluid ($W\ m^{-1}\ K^{-1}$)
L_b, L_t	block and reference lengths, respectively, in [29] (m)
N	number of perforations
$\overline{Nu}$	average Nusselt number in [29]
$Nu_D, \overline{Nu}_D$	local and average Nusselt
R_i	number, respectively, based on the fin thickness
P	air pressure (Pa)
$\dot{Q}$	heat dissipation rate from the fin (W)
Re	Reynolds number
Re_D	Reynolds number based on the fin thickness
Re^*	modified Reynolds number in [29]
R_i	Richardson number
T	temperature (K)
u, v, w	velocity components in X, Y and Z directions, respectively ($m\ s^{-1}$)
X, Y, Z	rectangular coordinates

Subscripts

DS, US	downstream and upstream, respectively
in	inlet
S	surface of the fin
SF, PF	solid and perforated fin, respectively
∞	free stream

Greek symbols

α	thermal expansion coefficient (T^{-1})
β	opening ratio in [29]
ε_{PF}	perforated fin effectiveness
μ	air viscosity ($kg\ m^{-1}\ s^{-1}$)
ρ	air density ($kg\ m^{-3}$)
Φ	porosity
τ_w	wall shear stress (Pa)

2. Problem description

Perforations like channels are considered through the length of fins. Fig. 1 illustrates the fin array configurations and the cross-section of perforations. Note that the fin in Fig. 1e has the highest both number of perforations (porosity) and enhanced heat transfer rate in [25]. Fins depicted in Fig. 1b–d have the same porosity of the fin in Fig. 1e but they have different numbers and sizes of perforations. Table 1 provides information about the perforated fins investigated in this study.

Incompressible air with constant properties in steady-state conditions flows over the faces of fins and inside the perforations. The Reynolds number based on the fin thickness, Re_D, changes from 100 to 350, corresponding to velocity of 0.37–1.28 m/s, which at this range, flow remains laminar around the fins.

The maximum corresponding Richardson number, $R_i = \frac{g\alpha\Delta T_{max}H}{V^2}$, at the smallest velocity (0.37 m/s) and the highest height is almost 0.12 and 0.096 for the exterior surfaces of fin and inside the perforation, respectively. Note that g is the gravitational acceleration, α is the thermal expansion coefficient $\left(\alpha = \frac{1}{0.5(25+70)+273}\right)$ that is calculated at the mean temperature of the inlet air and the fin base temperature, ΔT_{max} is the difference between inlet air temperature and fin base temperature, H is the characteristic length and V is the air velocity. The highest height used to calculate Richardson number is equal to the fin height (12 mm) for the exterior part of fin and the largest perforation height (9.6 mm) for inside the perforation. Therefore, the low values of Richardson numbers certify the dominance of forced convection in both exterior surfaces of fin and inside the perforation. Also, the fin material is aluminum with thermal conductivity of $202\ W\ m^{-1}\ K^{-1}$.

Since the flow is uniform and the configuration of the fin arrays is symmetrical, only one fin instead of entire the fin array is considered in the computational domain illustrated in Fig. 2 [22–25]. In Fig. 2, distances from the boundaries to the fin surfaces were obtained by several tests and by using the previous experiences in [22–26].

At Fig. 2, plane *abcd* is the inlet boundary and a uniform flow condition is considered for all variables using, $u_{in} = u_\infty$, $v_{in} = w_{in} = 0$ and $T_{in} = T_\infty = 298$ K. The similar conditions were applied for plane *bckj* as the free stream boundary. The zero gradient of variables in X direction, $\frac{\partial()}{\partial X} = 0$ was applied for plane *ijkl* as the outlet boundary that is far enough from the fin. Planes *abji* and *dckl* are symmetry planes so that the conditions of zero gradients in Z direction, $\frac{\partial()}{\partial Z} = 0$ and $w = 0$ have been applied for them. The remaining planes are wall and no-slip boundary condition was applied to them. Plane *efgh* as the fin base has a constant temperature of 343 K and planes *adeh* and *gfli* are adiabatic. In addition, since the maximum temperature difference at the computational domain is 45 K, the radiation heat transfer rate is less than 8% of the total heat transfer rate [27]; therefore, the effects of radiation heat transfer can be neglected appropriately.

3. Governing equations

Eqs. (1)–(3) describe the governing equations for a three-dimensional, incompressible steady-state laminar flow with constant properties, as follows:

Continuity equation:

$$\frac{\partial u_i}{\partial X_i} = 0 \tag{1}$$

Momentum equation:

$$\rho u_j \frac{\partial u_i}{\partial X_j} = -\frac{\partial P}{\partial X_i} + \mu \frac{\partial^2 u_i}{\partial X_i^2} \tag{2}$$

Energy equation:

$$\rho C_p u_j \frac{\partial T}{\partial X_j} = K \frac{\partial^2 T}{\partial X_i \partial X_i} \tag{3}$$

To calculate the temperature distribution inside solid parts of the fins, the conjugate problem of Fourier's steady-state heat conduction equation with convection in the fluid will be solved, simultaneously [24].

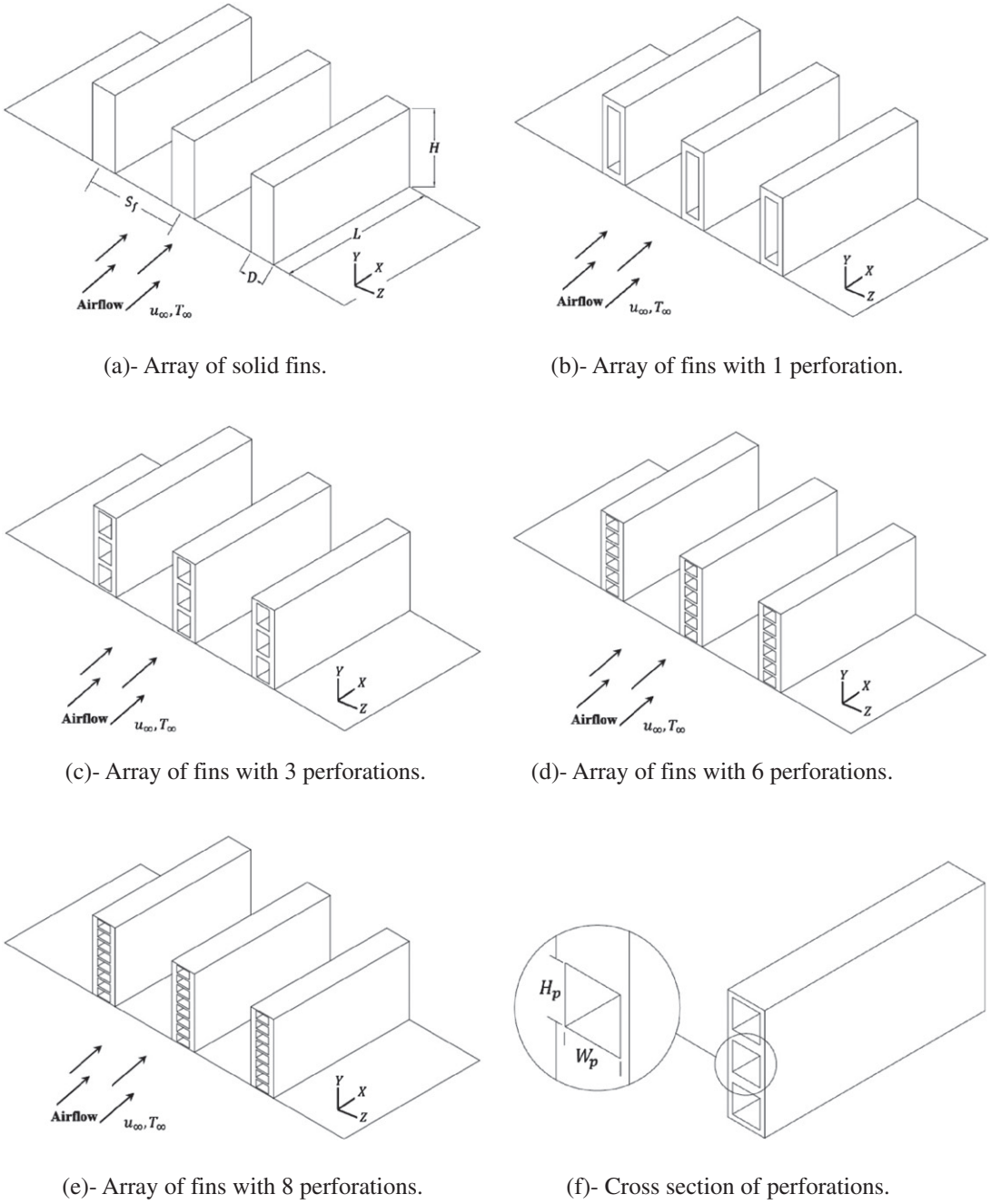

(a)- Array of solid fins.

(b)- Array of fins with 1 perforation.

(c)- Array of fins with 3 perforations.

(d)- Array of fins with 6 perforations.

(e)- Array of fins with 8 perforations.

(f)- Cross section of perforations.

Fig. 1. Configuration of fin arrays at the present study.

4. Grid generation and computational method

Computational results must be independent of the number of grid points [22–25]; therefore, for each fin, several computations were performed in such a manner that at each computation, the number of grid was increased. This procedure continues until an independency is obtained between the computational results and the number of grid points [22–25]. Table 2 shows a grid study to

Table 1
Geometry of various types of fins in laminar flow.

Number of perforation, N	Fin length, L (mm)	Fin height, H (mm)	Fin thickness, D (mm)	Fin spacing, S_f (mm)	Perforation width, W_p (mm)	Perforation height, H_p (mm)	Porosity (Φ)
0	24	12	4	20	0	0	0
1	24	12	4	20	2.22	9.6	0.44
3	24	12	4	20	2.22	3.2	0.44
6	24	12	4	20	2.22	1.6	0.44
8	24	12	4	20	2.22	1.2	0.44

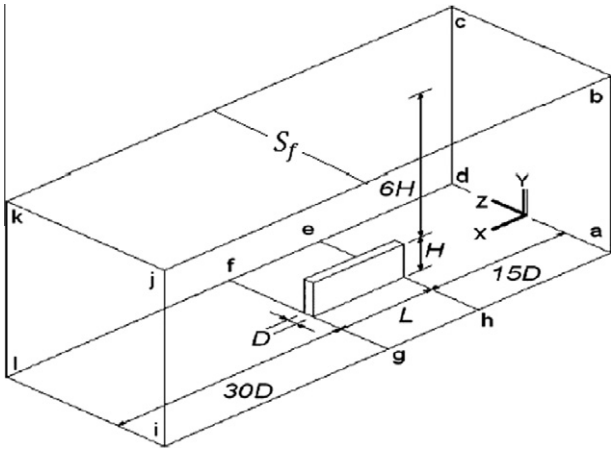

Fig. 2. Computational domain for arrays of fins in Fig. 1.

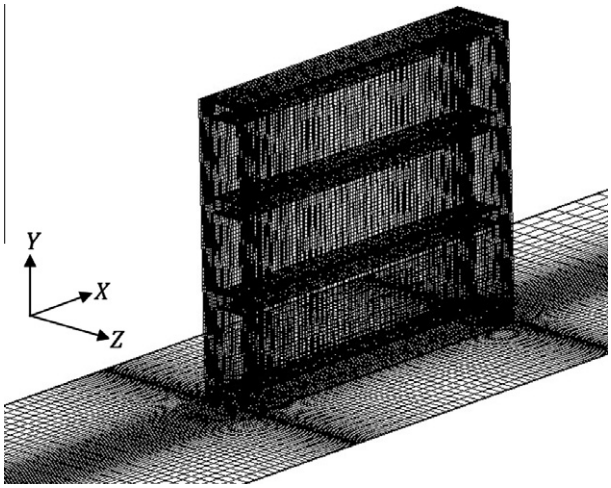

Fig. 3a. Three-dimensional view of grid structure for fin with three perforations.

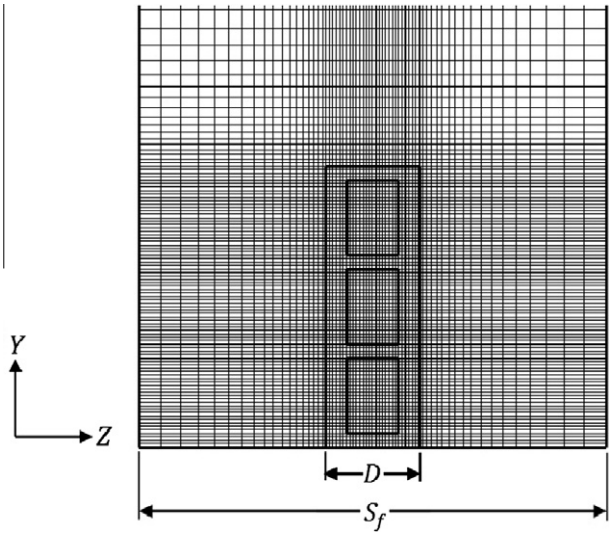

Fig. 3b. Two-dimensional view of grid structure for fin with three perforations.

obtain the proper number of grid points for the fin with three perforations.

According to Table 2, by increasing the number of grid points from Step 3 onwards, the maximum differences in average Nusselt numbers and friction drags are less than 1%. Therefore, to save both computation time and computer memory, the number of grid pints $180 \times 80 \times 40$ in X, Y and Z directions was selected, respectively, to simulate flow around the faces of fin with three perforations, as well as temperature distribution inside and outside the fin. The same procedure has been performed for other fins to obtain their corresponding appropriate number of grid points. Moreover, to capture the recirculation zone and reattachment point over the faces of fins accurately, grid points are considered dense near faces of the fins and perforations. Figs. 3a and 3b illustrate the grid structure for fin with three perforations.

The governing equations are discretized using a finite volume code with the second-order upwind scheme and are solved based on the SIMPLE algorithm proposed by Patankar [28]. An iterative line-by-line method was applied to solve the set of discretized equations by first solving continuity and momentum equations to determine the flow field around the faces of fins and inside the perforations. When the flow field is completely obtained, the energy equation is solved to determine the temperature distribution in the computational domain.

5. Validation

Although the developed numerical code in [25] used in the present study was validated with an experiment, its accuracy is again tested in this study. Since there is no experimental study regarding the perforated fins with structures like those in this study, only the numerical results of flow around a solid fin are compared with those of an experiment.

Table 2
Grid independent studies for the fin with three perforations at $Re_D = [350]$.

Step	Number of grids in whole domain (X, Y, Z)	Average Nusselt number, $\overline{Nu}_D$	Friction drag in flow direction (N)
1	$140 \times 50 \times 30$	2.86	2.68×10^{-5}
2	$160 \times 65 \times 35$	3.01	2.71×10^{-5}
3	$180 \times 80 \times 40$	3.21	2.75×10^{-5}
4	$190 \times 90 \times 50$	3.23	2.76×10^{-5}
5	$200 \times 95 \times 55$	3.24	2.76×10^{-5}
6	$210 \times 100 \times 60$	3.24	2.77×10^{-5}

Nakamura and Igarashi [29] experimentally investigated forced convection heat transfer from a block located in the center of a rectangular duct. The block was 45 mm in length, 45 mm in width, and 2 mm in height, and the length, width and height of the duct were 235 mm, 200 mm and 10 mm, respectively. Also, the upstream distance was 77.5 mm. Fig. 4 illustrates the position of the block inside the duct. The mean velocity of air at upstream of the block was in the range of $u_\infty = 0.24$–$0.72\ \mathrm{m\ s^{-1}}$ and flow remained completely laminar and fully developed at the length of channel. Nakamura and Igarashi [29] experimentally measured heat transfer characteristics of the block at both constant heat flux and constant wall temperature, and they defined the opening ratio:

$$\beta = 1 - \frac{H_b}{H_d} \tag{4}$$

Based on the opening ratio, Nakamura and Igarashi [29] introduced a modified Reynolds number in their experiment:

$$Re^* = \frac{\rho u_\infty L_t}{\beta^2 \mu} \tag{5}$$

where L_t is the reference length, either hydraulic diameter of the duct or block length.

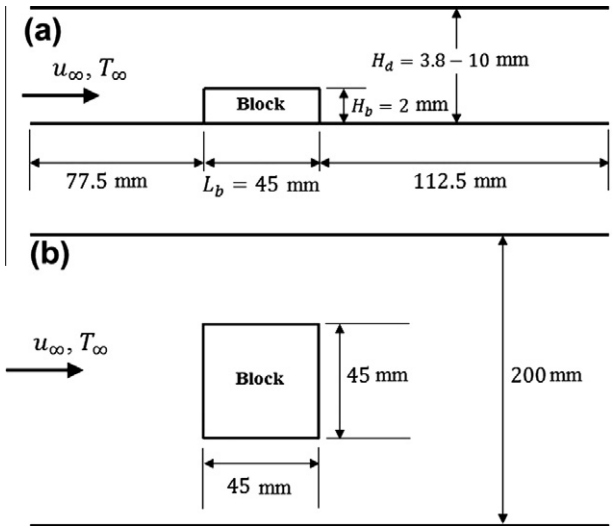

Fig. 4. Position of the block inside the duct in the experiment of [29]. (a): side view, (b): top view. (This figure is reproduced here by the kind permission of publisher of [29].)

The same conditions in the experiment were considered in this study to validate the developed numerical code. Fig. 5 compares the average Nusselt numbers in simulation and experiment for the block in different Re^* and β. In Fig. 5, the modified Reynolds number is defined based on the hydraulic diameter of the duct. The average Nusselt number in [29] is obtained as follows:

$$\overline{Nu} = \frac{\bar{h}L_b}{K} \tag{6}$$

According to Fig. 5, in this study, the acceptable agreements between the results of the present simulation with those of the experiment of [29] verify accuracy of the developed numerical code.

6. Results and discussion

This section presents the Laminar convective heat transfer characteristics of arrays of perforated fins in the range of Re_D = 100–350. Perforations are along the length of fins and their numbers vary from 1 to 8 at a constant porosity. Due to perforations, a part of the flow enters inside the perforations; therefore, the fin area that is touched by fluid increases in a perforated fin compared with a solid fin. This area can be obtained as:

$$A_F = 2H \times L + D \times L + 2N \times L \times H_P + 2N \times L \times W_P \tag{7}$$

Based on Eq. (7), the fin area touched by the air becomes larger by an increase in the number of perforations. Consequently, friction drag not only is larger in a perforated fin compared with a solid fin, but also increases by adding the number of perforations. Friction drag can be obtained as:

$$F_F = \sum(\tau_w)_i \Delta A_i = \sum \mu \left(\frac{\partial u}{\partial n_i}\right) \Delta A_i \tag{8}$$

where τ_w is the wall shear stress over the entire face of each fins and perforation.

However, a solid fin has a larger frontal area in flow direction compared with a perforated fin; therefore, the pressure drag is expected to be larger in a solid fin with respect to a perforated fin. In addition, since the frontal area is the same for all the perforated fins in this study, the pressure drag remains almost the same among all the perforated fins. The frontal area and the pressure drag can be obtained by the following relations [22–24]:

$$A_P = D \times H - N \times H_P \times W_P \tag{9}$$

$$F_P = \left(-\sum P_i \Delta A_i\right)_{US} - \left(-\sum P_i \Delta A_i\right)_{DS} \tag{10}$$

The total drag is consists of both friction and pressure drag; therefore, the total drag in flow direction is obtained as:

$$F_D = F_F + F_P \tag{11}$$

Fig. 6a–6c illustrates friction, pressure and total drag in flow direction for all types of fins at different Reynolds numbers.

Based on Figs. 6a and 6b, the considerable differences between friction and pressure drag of a solid fin and that of a perforated fin is apparent. Also, according to Fig. 6a, due to the low velocity of air inside the perforations, the difference in friction drag among perforated fins is negligible at low Reynolds numbers; however, at the higher Reynolds numbers a slight difference in friction drag among perforated fins can be detected.

Moreover, the effects of friction and pressure drags indicate how the total drag remains almost the same among all types of fins. In other words, perforated fins do not affect total drag.

Eq. (12) describes the Nusselt number that represents the heat transfer characteristics of an object.

$$Nu_D = \frac{hD}{K} \tag{12}$$

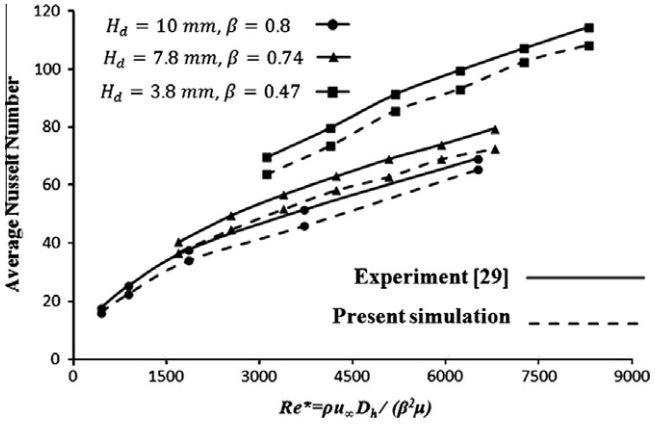

Fig. 5. Comparison of the numerical and experimental average Nusselt numbers around a block. (Some parts of this figure are reproduced by the kind permission of publisher of [29].)

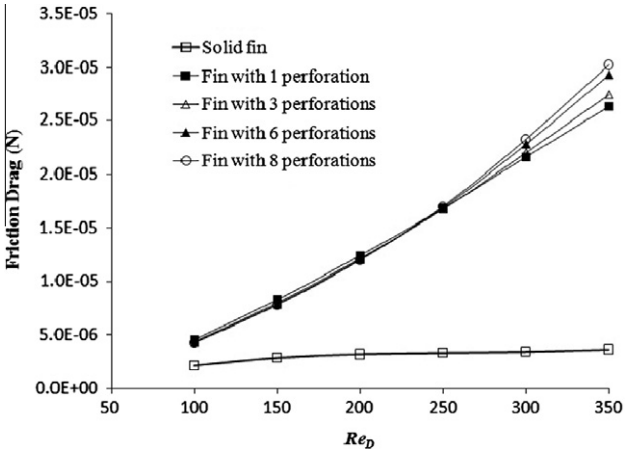

Fig. 6a. Variation of friction drag in flow direction for various types of fins.

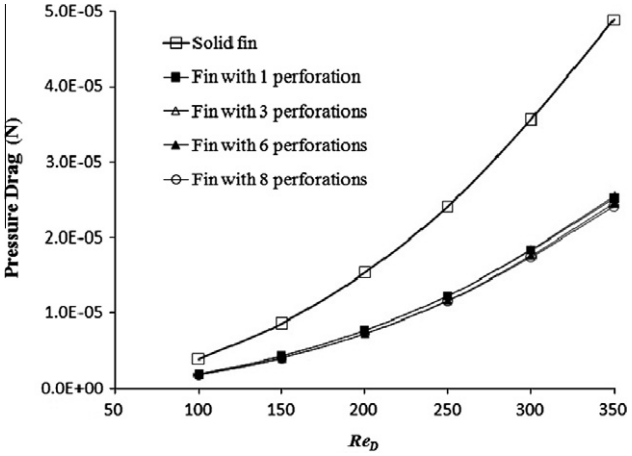

Fig. 6b. Variation of pressure drag in flow direction for various types of fins.

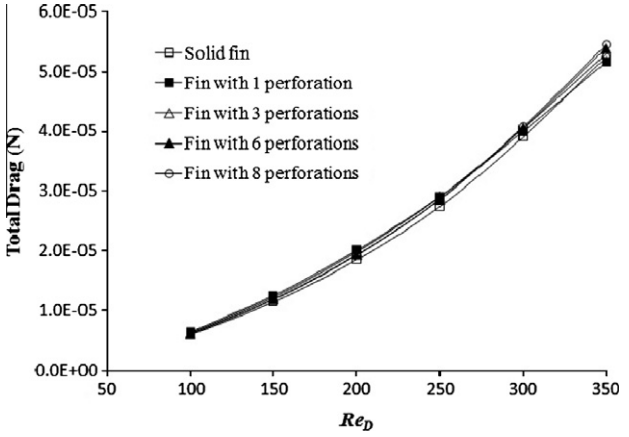

Fig. 6c. Variation of total drag in flow direction for various types of fins.

Although the authors of [25] used the average Nusselt numbers of different kinds of fins, since the fin areas that are touched by the air are different among the solid and perforated fins, it is better to use the local distribution of Nusselt number instead of the average Nusselt number. Fig. 7 illustrates the local distribution of Nusselt number at the inner surfaces of perforations of two perforated fins in flow direction.

According to Fig. 7, the thermal entrance length of each perforation of a fin with smaller number of perforations is much higher than that of each perforation of a fin with larger number of perforations. Therefore, it is expected that between two perforated fins with the same porosity, the one with smaller number of perforation is able to enhance the heat transfer rate more than another fin.

To further investigate the heat transfer characteristics of the perforated fins, perforated fin effectiveness (PFE), the parameter defined by Shaeri and Yaghoubi [25], is used. Perforated fin effectiveness represents the percentage of increase in heat transfer rate with respect to a solid fin by using a perforated fin. This non-dimensional parameter is shown mathematically as follows:

$$\varepsilon_{PF} = \frac{\dot{Q}_{PF} - \dot{Q}_{SF}}{\dot{Q}_{SF}} \times 100 \tag{13}$$

where $\dot{Q}$ is the heat dissipation rate from the fin and can be calculated by the following relation [24]:

$$\dot{Q} = \sum h_i \Delta A_i (T_S - T_\infty) \tag{14}$$

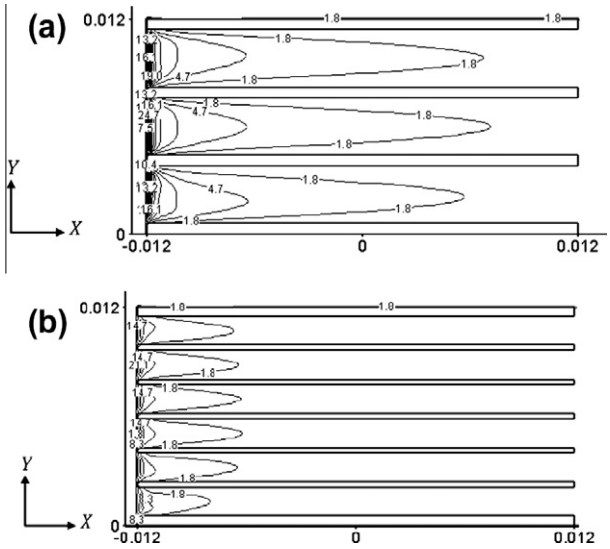

Fig. 7. Distribution of local Nusselt number in flow direction at $Re_D = 350$ for perforated fins with (a): three perforations and (b): six perforations.

Fig. 8 compares perforated fin effectiveness of perforated fins at different Reynolds numbers.

Based on Fig. 8, at a specific porosity, by a decrease in the number of perforations (increase in the perforation sizes), the enhanced heat transfer rate increases significantly such that a fin with one perforation enhances the heat transfer rate almost 80% at $Re_D = 350$. However, the fin with eight perforations that had the highest heat transfer enhancement in [25] has the maximum PFE equal to 35%. This conclusion is completely compatible with the local distribution of Nusselt number in Fig. 7.

In addition, in low Reynolds numbers, fins with more perforations are not so powerful in order to enhance the heat transfer rate, while fins with a smaller number of perforations increase the heat transfer rate considerably, even in low Reynolds numbers.

Saving primary materials of the fins is another important advantage of using the proposed perforated fins in this study in such a manner that using such perforated fins reduces the weight of the solid fins by 44%. Therefore, by using the proposed perforated fins in this study, two objectives of fin optimization can be met.

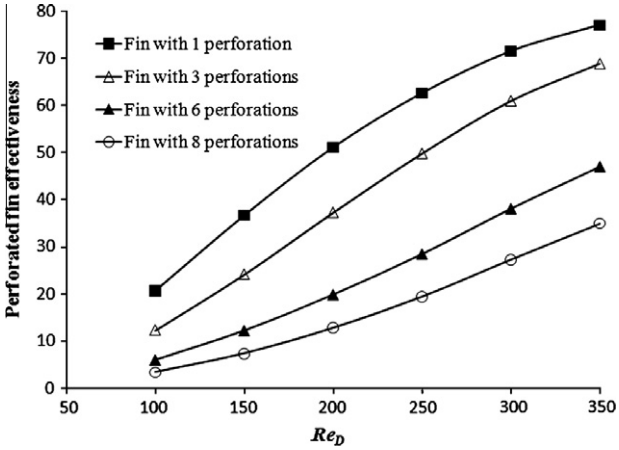

Fig. 8. Variation of perforated fin effectiveness.

7. Conclusions

In [25], the authors increased the number of perforations (porosity) and reported that the heat transfer enhancement has a direct relation with the porosity. In this study, the fin with the highest porosity in [25] was selected and without change of its porosity, the number and sizes of its perforations were varied to investigate the effects of perforation sizes on laminar heat transfer characteristics of the fin. The obtained results are as the follows:

(a) Between two perforated fins at the same porosity, the one with more perforations has the higher friction drag due to having more floors and ceilings because of the extra perforations. However, since the velocity in laminar flow is low inside the perforations, the difference in friction drag is not sensible in low Reynolds numbers between two perforated fins at the same porosity.
(b) Due to the same frontal area for all perforated fins, the pressure drag remains almost the same among all perforated fins.
(c) Total drag, including both friction and pressure drags remains almost unchanged among all types of fins, including solid and perforated fins.
(d) At the same porosity, the thermal entrance length of each perforation of a fin with a smaller number of perforations is larger than that of each perforation of a fin with a larger number of perforations.
(e) At the same porosity, the perforated fins with a smaller number of perforations (larger in perforation sizes) enhance the heat transfer rate more efficiently in such a manner that by using perforated fins with one perforation, the heat transfer rate is enhanced nearly 80%.

Acknowledgments

The authors wish to thank Professor Hajime Nakamura in the Department of Mechanical Engineering, National Defense Academy, Hashirimizu, Yokosuka, Japan, for providing us with the experimental data.

References

[1] Malekzadeh P, Rahideh H, Karami G. Optimization of convective–radiative fins by using differential quadrature element method. Energy Convers Manage 2006;47:1505–14.
[2] Badescu V. Optimum fin geometry in flat plate solar collector systems. Energy Convers Manage 2006;47:2397–413.
[3] Kundu B, Das PK. Performance analysis and optimization of elliptic fins circumscribing a circular tube. Int J Heat Mass Transfer 2007;50:173–80.
[4] Malekzadeh P, Rahideh H, Setoodeh AR. Optimization of non-symmetric convective-radiative annular fins by differential quadrature method. Energy Convers Manage 2007;48:1671–7.
[5] Kundu B, Das PK. Performance and optimum dimensions of flat fins for tube-and-fin heat exchangers: a generalized analysis. Int J Heat Fluid Flow 2009;30:658–68.
[6] Aziz A, Beers-Green AB. Performance and optimum design of convective-radiative rectangular fin with convective base heating, wall conduction resistance, and contact resistance between the wall and the fin base. Energy Convers Manage 2009;50:2622–31.
[7] Hong F, Cheng P. Three dimensional numerical analyses and optimization of offset strip-fin microchannel heat sinks. Int Commun Heat Mass Transfer 2009;36:651–6.
[8] Zhang X, Liu D. Optimum geometric arrangement of vertical rectangular fin arrays in natural convection. Energy Convers Manage 2010;51:2449–56.
[9] Azarkish H, Sarvari SMH, Behzadmehr A. Optimum geometry design of a longitudinal fin with volumetric heat generation under the influences of natural convection and radiation. Energy Convers Manage 2010;51:1938–46.
[10] Kundu B, Bhanja D. Performance and optimization analysis of a constructal T-shaped fin subject to variable thermal conductivity and convective heat transfer coefficient. Int J Heat Mass Transfer 2010;53:254–67.
[11] Kim D-K, Jung J, Kim SJ. Thermal optimization of plate-fin heat sinks with variable fin thickness. Int J Heat Mass Transfer 2010;53:5988–95.
[12] Hajabdollahi F, Hashemipour Rafsanjani H, Hajabdollahi Z, Hamidi Y. Multi-objective optimization of pin fin to determine the optimal fin geometry using genetic algorithm. Appl Math Model 2012;36:244–54.
[13] Kiwan S, Al-Nimr MA. Using porous fins for heat transfer enhancement. J Heat Transfer 2001;123:790–5.
[14] Kiwan S. Thermal analysis of natural convection porous fins. Transport Porous Med 2007;67:17–29.
[15] Kiwan S. Effect of radiative losses on the heat transfer from porous fins. Int J Therm Sci 2007;46:1046–55.
[16] Kundu B, Bhanja D. An analytical prediction for performance and optimum design analysis of porous fins. Int J Refrig 2011;34:337–52.
[17] Souidi N, Bontemps A. Countercurrent gas–liquid flow in plate-fin heat exchangers with plain and perforated fins. Int J Heat Fluid Flow 2001;22:450–9.
[18] Sara ON, Pekdemir T, Yapici S, Yilmaz M. Heat-transfer enhancement in a channel flow with perforated rectangular blocks. Int J Heat Fluid Flow 2001;22:509–18.
[19] Sahin B, Demir A. Performance analysis of a heat exchanger having perforated square fins. Appl Therm Eng 2008;28:621–32.
[20] Sahin B, Demir A. Thermal performance analysis and optimum design parameters of heat exchanger having perforated pin fins. Energy Convers Manage 2008;49:1684–95.
[21] Karabacak R, Yakar G. Forced convection heat transfer and pressure drop for a horizontal cylinder with vertically attached imperforate and perforated circular fins. Energy Convers Manage 2011;52:2785–93.
[22] Shaeri MR, Yaghoubi M, Jafarpur K. Heat transfer analysis of lateral perforated fin heat sinks. Appl Energy 2009;86:2019–29.
[23] Yaghoubi M, Shaeri MR, Jafarpur K. Three-dimensional numerical laminar convection heat transfer around lateral perforated fins. Comput Therm Sci 2009;1:323–40.
[24] Shaeri MR, Yaghoubi M. Numerical analysis of turbulent convection heat transfer from an array of perforated fins. Int J Heat Fluid Flow 2009;30:218–28.
[25] Shaeri MR, Yaghoubi M. Thermal enhancement from heat sinks by using perforated fins. Energy Convers Manage 2009;50:1264–70.
[26] Rouvreau S, David L, Calluaud D, Joulain P. Laminar junction flow at low Reynolds number: influence W_p of the upstream region on the comparison between experiments and calculations. C. R. Mecanique 2005;333:265–72.
[27] Leung CW, Probert SD. Heat-exchanger performance. Effect of orientation. Appl Energy 1989;33:235–52.
[28] Patankar SV. Numerical heat transfer and fluid flow. Washington, DC: Hemisphere; 1980.
[29] Nakamura H, Igarashi T. Forced convection heat transfer from a low-profile block simulating a package of electronic equipment. J Heat Transfer 2004;126:463–70.